

DNA, 0.5 mg/ml acetylated BSA and 1× manufacturer-recommended hybridization buffer in a 45 °C rotisserie oven for 16 h. Washing and staining were performed in a GeneChip Fluidics Station (Affymetrix) using the appropriate antibody amplification, washing and staining protocols. The phycoerythrin-stained arrays were scanned as digital image files, which were analyzed with GeneChip Operating Software (Affymetrix). The expression data were converted to copy numbers of mRNA per cell by the Percelemo method, quality controlled, and analyzed using Percelemo software (Kanno et al., 2006). The GeneChip data have been deposited in the NCBI Gene Expression Omnibus (GEO; <http://www.ncbi.nlm.nih.gov/geo/>) and is accessible through GEO series accession number GSE 10796.

Quantitative real-time RT-PCR

Quantitative real-time PCR was performed to confirm the results of GeneChip analysis. RNAs from E11.5 and E14.5 NPCs were reverse transcribed using Superscript II (Invitrogen) and amplified by PCR, with a specific pair of primers for each gene, using the Mx3000P system (Stratagene, La Jolla, CA, USA). The expression of target genes was normalized to that of glyceraldehyde-3-phosphate dehydrogenase (*Gapdh*). The gene-specific primers were as follows: mouse *N-myc*: N-myc-S, 5'-aacatgctgcaccct-cacc-3'; N-myc-AS, 5'-tagcaagtccgagcgtgttc-3'; mouse *Hmga2*: Hmga2-S, 5'-ggcagccgtccacatcag-3'; Hmga2-AS, 5'-taatcctcctc-gggactc-3'; mouse *Sox11*: Sox11-S, 5'-gagcctgtagcagaagtcg-3'; Sox11-AS, 5'-tgaacaccaggtcggagaag-3'; mouse *Bhlhb5*: Bhlhb5-S, 5'-gttgccctcaacatcaac-3'; Bhlhb5-AS, 5'-acttttgca-gaggctggac-3'; mouse *Bcl11a*: Bcl11a-S, 5'-gcatcaagctggagaag-gag-3'; Bcl11a-AS, 5'-gagctccatccgaaactg-3'; mouse *Gapdh*: Gapdh-S, 5'-accacagctccatccatc-3'; Gapdh-AS, 5'-tccaccac-cctgtgctgta-3'.

In situ hybridization

Digoxigenin- (DIG; Roche) labeled cRNA probes were synthesized for each gene, following the manufacturer's instructions. Cryosections were washed with PBS and fixed with 4% PFA. After fixation, sections were incubated in prehybridization solution (5× sodium chloride sodium citrate (SSC), 1% SDS, 50 μg/ml yeast transfer RNA, 50 μg/ml heparin in 50% formamide) at 70 °C for 1 h and hybridized with 500 ng/ml of DIG-labeled cRNA probes at 65 °C for 16 h. After three washes with wash solution 1 (5× SSC, 1% SDS in 50% formamide) and wash solution 2 (2× SSC in 50% formamide), sections were blocked with 10% normal sheep serum in TBST at room temperature for 1 h and then incubated with 1:1000 alkaline phosphatase-conjugated anti-DIG antibody (Roche) at 4 °C for 16 h. After four washes with TBST, hybridized probes were visualized with 5-bromo-4-chloro-3 indolylphosphate and nitro blue tetrazolium chloride.

Recombinant retrovirus construction and infection

Human *N-myc* and mouse *Hmga2* cDNAs were cloned into the expression vector pMys, which contains an internal ribosome entry site followed by the region upstream of the *EGFP* gene (Morita et al., 2000). The Plat-E packaging cell line was transiently transfected with the retrovirus DNA by Trans-IT 293 (Mirus, Madison, WI, USA) (Morita et al., 2000). On the following day, the medium was replaced with N2/DME/F12/bFGF, and the cells were cultured in this medium for 1 day before virus was collected.

Fluorescence activated cell sorting

Virus-infected E11.5 NPCs were cultured for 4 days, after which GFP-labeled cells were sorted using a FACS Vantage (Becton Dickinson, Franklin Lakes, NJ, USA) at a flow rate of less than 1500 events/s; gating parameters were set by side and forward

scatter to eliminate debris, dead and aggregated cells. After sorting, genomic DNA was extracted and used for bisulfite sequencing.

Bisulfite sequencing

Sodium bisulfite treatment of genomic DNA was performed using a Methylamp DNA Modification kit (Epigentek, Brooklyn, NY, USA), according to the manufacturer's instructions. The region in the *gfap* promoter containing the STAT-binding site of the bisulfite-treated genomic DNA was amplified by PCR using the following primers: GFM5 (5'-GGGATTATTAGGAGAATTTAGAAAGTAG-3'), GFMas (5'-TCTACCCATTCTAAACTTCTAATATCTAC-3'). The PCR products were cloned into pT7Blue vector (Novagen, Madison, WI, USA) and at least 12 randomly selected clones were sequenced.

RESULTS

Preparation of NPCs from different developmental stages and comparison of their gene expression profiles by GeneChip analysis

E11.5 NPCs do not differentiate into astrocytes, even in the presence of the astrocyte-inducing cytokine LIF, in contrast to 4-day cultured E14.5 NPCs (Takizawa et al., 2001). As a first step toward identifying factors involved in the inhibition of astrocyte differentiation of NPCs at mid-gestation, we examined the gene expression profiles of E11.5 and E14.5 NPCs.

E11.5 and E14.5 NPCs were isolated from embryonic telencephalon and cultured as indicated in Fig. 1A. To evaluate the purity of NPCs in each cell population, the cells were stained with antibody against SOX2, an NPC marker (Graham et al., 2003). As shown in Fig. 1B and C, the majority of cells in both populations were positive for SOX2, indicating that NPCs were highly enriched. An Affymetrix mouse genome GeneChip array was chosen to compare expression profiles in the two populations, and we adopted the Percelemo method to normalize gene expression from different samples (Kanno et al., 2006). The method enabled us to quantify mRNA molecules per cell based on the measurement of cell by adding a grade-dosed spike cocktail to the samples. We excluded genes whose transcript copy number was below six per cell. Scatter plots illustrating the differences between E11.5 and E14.5 NPCs are shown in Fig. 1D; 194 genes were expressed at >fivefold higher level in E11.5 NPCs than in E14.5 NPCs (Fig. 1D, light blue zone). Of these, 102 were known genes, and were classified by functional category (Fig. 1E). Since we wished to identify negative regulators of astrocyte differentiation, or factors involved in the epigenetic modification in midgestational NPCs, we focused on transcription-related genes (Fig. 1E, red). These 21 genes are listed in Table 1, and five (*N-myc*, *Hmga2*, *Bhlhb5*, *Sox11*, *Bcl11a*) were selected for further analysis because they have been reported to play roles in cell growth, differentiation, and chromatin remodeling in other types of stem cells (Sawai et al., 1990; Zhou et al., 1995; Saiki et al., 2000; Knoepfler et al., 2002; Brunelli et al., 2003; Sock et al., 2004).

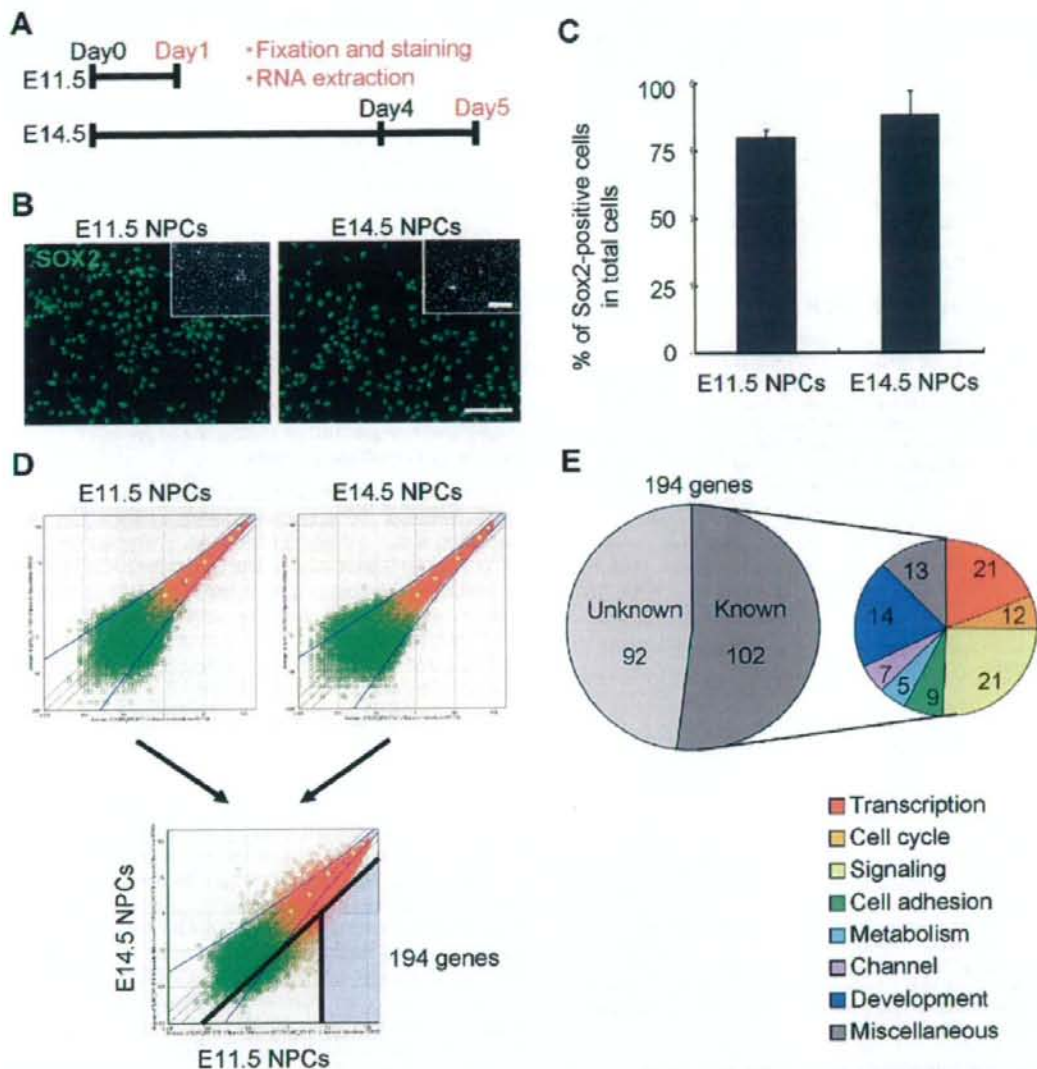


Fig. 1. Comparison of gene expression profiles in E11.5 and E14.5 NPCs. (A) Schematic of experimental protocol. NPCs isolated from E11.5 mouse telencephalon were plated (day 0) and used on the following day for immunostaining and RNA extraction (day 1). NPCs isolated at E14.5 were expanded for 4 days and replated on day 4. On day 5, these cells were fixed for immunostaining. RNA was also extracted. (B) E11.5 and E14.5 NPCs were stained with antibody against Sox2 (green). Scale bar=25 μ m. Insets: Hoechst nuclear staining of each field. Scale bar=25 μ m. (C) The percentage of Sox2-positive cells in E11.5 and E14.5 NPCs was quantified. Mean \pm S.D. (D) Scatter plots of E11.5 (upper left) and E14.5 (upper right) samples obtained from GeneChip analysis indicated no significant change between independent experiments with the same sample. Overview (lower plot) of gene expression change was compared between each sample. One hundred ninety-four genes were expressed at >fivefold higher level in E11.5 NPCs than E14.5 NPCs (light blue zone). (E) Of the 194 genes that were highly expressed in E11.5 NPCs, known genes were classified according to Affymetrix gene ontology. For interpretation of the references to color in this figure legend, the reader is referred to the Web version of this article.

Table 1. Transcription-related genes highly expressed in E11.5 NPCs

Probe set ID	GenBank ID	Gene symbol	E11.5 NPCs	E14.5 NPCs	E11.5/E14.5
1433919_at	AV302111	<i>Asb4</i>	9.8	0.5	19.6
1419406_a_at	NM_016707	<i>Bcl11a</i>	13.8	1.8	7.7
1418271_at	NM_021560	<i>Bhlhb5</i>	10.6	1.2	8.8
1452207_at	Y15163	<i>Cited2</i>	16.7	2.6	6.4
1449470_at	NM_010053	<i>Dlx1</i>	13.8	2.4	5.8
1448877_at	NM_010054	<i>Dlx2</i>	9.8	1.8	5.4
1449863_a_at	NM_010056	<i>Dlx5</i>	11.2	0.7	16.0
1459211_at	AW546128	<i>Gli2</i>	8.0	1.5	5.3
1456067_at	AW546010	<i>Gli3</i>	20.6	2.1	9.8
1422851_at	X58380	<i>Hmga2</i>	25.5	0.5	51.0
1450723_at	BQ176915	<i>Ilis1</i>	8.6	0.1	86.0
1427300_at	D49658	<i>Lhx8</i>	10.5	0.1	105.0
1417155_at	BC005453	<i>N-myc</i>	8.2	1.2	6.8
1415811_at	BB702754	<i>NP95</i>	12.6	2.1	6.0
1421193_a_at	NM_016768	<i>Pbx3</i>	12.3	1.6	7.7
1417400_at	NM_030690	<i>Rai14</i>	11.0	1.6	6.9
1435856_x_at	AV310148	<i>Smcarb1</i>	8.0	1.6	5.0
1431255_at	BB656631	<i>Sox11</i>	38.7	6.2	6.2
1450034_at	AW214029	<i>Stat1</i>	9.6	1.8	5.3
1416711_at	NM_009322	<i>Tbr1</i>	9.8	0.2	49.0
1423424_at	BB732077	<i>Zic3</i>	11.2	0.5	22.4

Genes reported to participate in cell growth, differentiation and chromatin remodeling are shown in boldface.

Spatio-temporal expression patterns of genes highly expressed in E11.5 NPCs

To substantiate the GeneChip results, we extracted RNA from E11.5 and E14.5 NPCs and performed real-time RT-PCR using specific primers for each selected gene. Consistent with the GeneChip analysis, all five genes were highly expressed in E11.5 NPCs compared with E14.5 NPCs (Fig. 2A). We next performed *in situ* hybridization for each gene using E11.5, E14.5 and E17.5 mouse brain sections (Fig. 2B). *N-myc* and *Hmga2* mRNAs were specifically detected in the ventricular zone (VZ) of E11.5 brain, implying that *N-myc* and *Hmga2* play some role in NPCs at this stage. By contrast, *Bhlhb5*, *Sox11* and *Bcl11a* expression was stronger in cortical plate, where postmitotic neurons reside, than in the VZ (Fig. 2B). We therefore decided to analyze the function of *N-myc* and *Hmga2* in more detail.

Transduction of *N-myc* and *Hmga2* inhibits astrocyte differentiation of E14.5 NPCs

We next examined whether *N-myc* and *Hmga2* affect astrocyte differentiation of NPCs. We expressed EGFP alone (control), and EGFP together with either *N-myc* or *Hmga2*, using retroviral infection in E14.5 NPCs, in which expression of the endogenous genes is very low. Virus-infected E14.5 NPCs were cultured for 4 days in the presence of LIF to induce astrocyte differentiation, and then stained with antibodies against GFP and GFAP. As shown in Fig. 3A and B, NPCs infected with control virus effectively differentiated into GFAP-positive astrocytes in response to LIF stimulation ($42 \pm 2.6\%$). In contrast, GFAP-positive astrocyte differentiation was virtually abolished in cells ec-

topically expressing *N-myc* ($0.5 \pm 0.4\%$) and *Hmga2* ($3 \pm 2.0\%$) (Fig. 3A, B). Expression of these genes did not significantly affect neuronal differentiation of NPCs, as assessed by monitoring expression of the neuronal marker β III-tubulin, compared with the control cells (Fig. 3C, D). We further examined whether the observed suppression of astrocyte differentiation of NPCs infected with viruses encoding *N-myc* or *Hmga2* could be attributed to specific cell-growth inhibition or to cell death. To address this issue, we performed immune staining for the cycling cell marker Ki67 and the apoptotic marker cleaved caspase 3. Although proliferation of NPCs ectopically expressing *N-myc* or *Hmga2* appeared to be slightly enhanced, expression of either gene caused negligible cell death. These results suggest that *N-myc* and *Hmga2* inhibit astrocyte differentiation of NPCs by a mechanism distinct from that of the neurogenic bHLH factors, which enhance neuronal differentiation (Sun et al., 2001).

Continuous expression of *N-myc* and *Hmga2* in E11.5 NPCs fails to preserve the hypermethylated status of an astrocyte-specific gene promoter

We have previously shown that the *gfap* promoter is highly methylated in E11.5 NPCs, and becomes demethylated as gestation proceeds (Takizawa et al., 2001). This demethylation enables NPCs at later developmental stages, E14.5 or thereafter, to respond to LIF and differentiate into GFAP-positive astrocytes. As shown in the foregoing data, expression levels of *N-myc* and *Hmga2* thus seemed to be reduced concurrently with the developmental stage-dependent demethylation of an astrocyte-specific gene promoter; furthermore, ectopic expression of these genes in E14.5 NPCs inhibited GFAP-positive astrocyte differentiation. We therefore hypothesized that sustained expression of *N-myc* and *Hmga2* in E11.5 NPCs might maintain the hypermethylated status of the *gfap* promoter. To test this, we infected E11.5 NPCs with viruses expressing EGFP alone and EGFP together with either *N-myc* or *Hmga2* and cultured them for 4 days. GFP-positive cells were sorted by FACS and their genomic DNAs were extracted for bisulfite sequencing. As observed in the previous study (Takizawa et al., 2001), the *gfap* promoter including the STAT3 site became demethylated to about 65% in control virus-infected cells after the 4-day culture, and this was also the case for both *N-myc*- and *Hmga2*-expressing virus-infected cells (Fig. 3E, F). These results indicate that sustained expression of *N-myc* and *Hmga2* in E11.5 NPCs does not affect the process of demethylation in this astrocyte-specific gene promoter. On the other hand, when 4-day-cultured control virus-infected E11.5 NPCs were then stimulated with LIF for an additional 4 days, GFAP-positive astrocytes appeared, probably due to demethylation in the promoter, whereas neither *N-myc* nor *Hmga2* virus-infected cells gave rise to astrocytes even in the presence of LIF (data not shown). These results suggest that *N-myc* and *Hmga2* inhibit precocious astrocyte differentiation of midgestational NPCs independent of the DNA methylation status of an astrocyte-specific gene promoter.

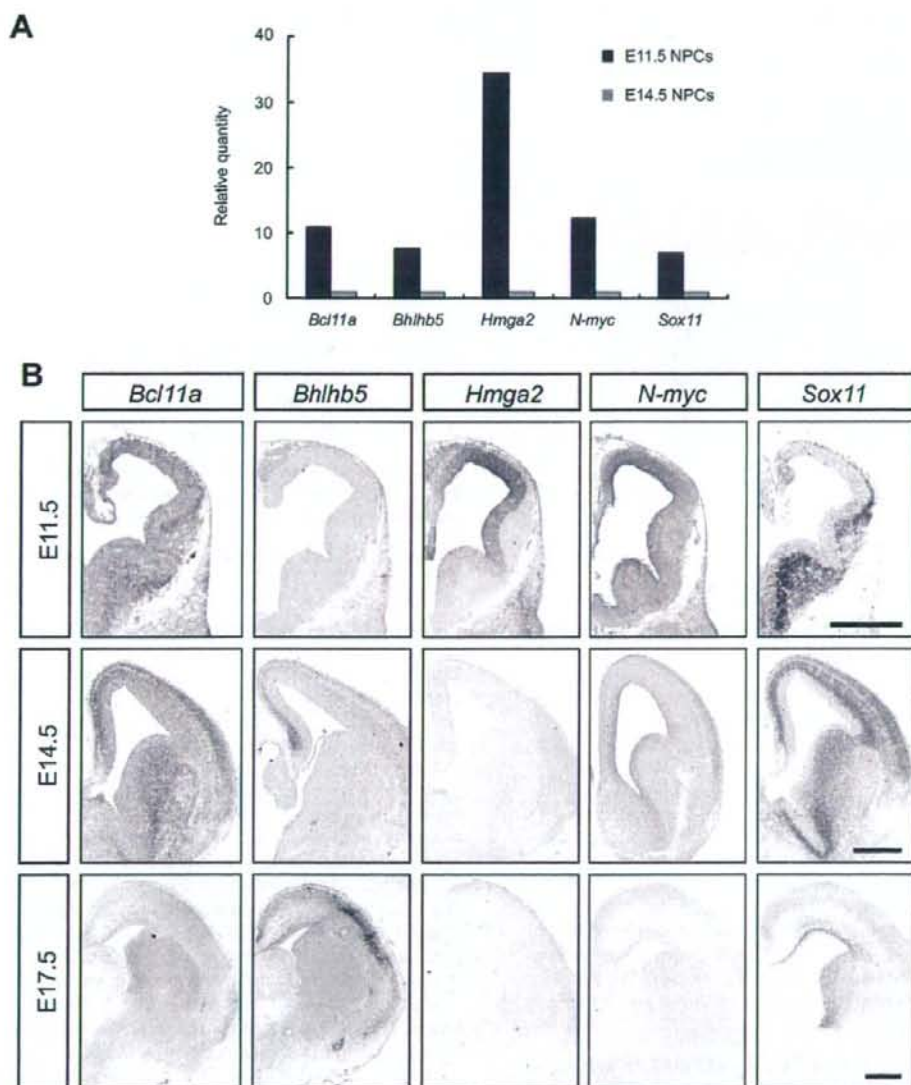


Fig. 2. *N-myc* and *Hmga2* are highly expressed in the VZ of E11.5 mouse brain. (A) Gene-specific real-time RT-PCR was performed to validate GeneChip analysis data. (B) *In situ* hybridization was performed for E11.5, E14.5 and E17.5 mouse brain sections. No signal was detected when sense-probes for each gene were used (data not shown). Scale bar=500 μ m.

DISCUSSION

In this study, we compared NPC gene expression profiles at different developmental stages using Affymetrix GeneChips and the Percellome method, and then analyzed by *in situ* hybridization the spatio-temporal expression patterns of genes which were highly expressed in E11.5 NPCs. We found that *N-myc* and *Hmga2* were specifically expressed in E11.5 NPC both *in vivo* and *in vitro* and,

furthermore, that the transduction of these genes into NPCs suppressed LIF-induced astrocytic differentiation without affecting DNA demethylation of the astrocyte-specific *gfap* gene promoter.

The basic HLH leucine zipper transcription factor *N-myc*, a member of the *myc* family of oncogenes, is a nuclear phosphoprotein exhibiting site-specific DNA-binding activity (Ramsay et al., 1986; Alex et al., 1992), and has

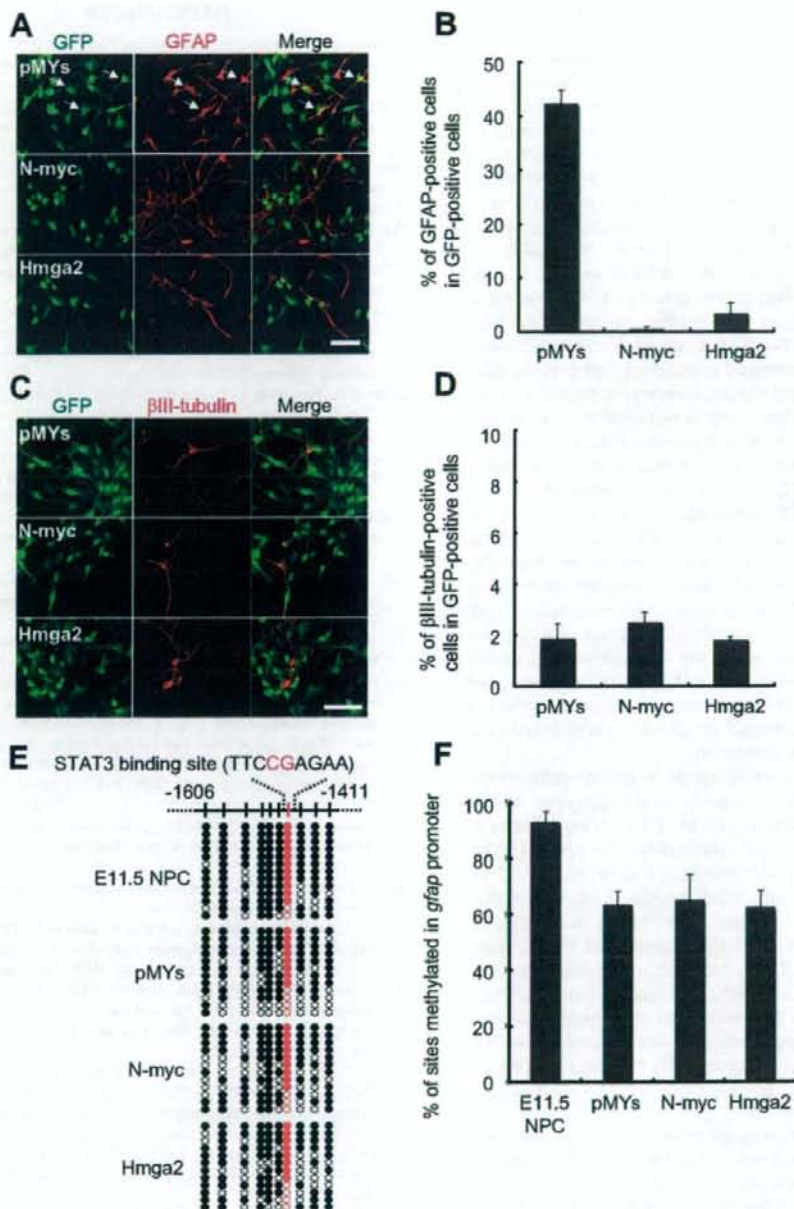


Fig. 3. N-myc and Hmga2 inhibit astrocyte differentiation of NPCs even in the presence of LIF. (A–D) E14.5 NPCs were infected with recombinant retroviruses engineered to express *EGFP* alone (pMYs), and *EGFP* together with either *N-myc* (N-myc) or *Hmga2* (Hmga2), and cultured with LIF (50 ng/ml) for 4 days to induce astrocyte differentiation. The cells were then stained with antibodies against GFP (green) and GFAP (red) (A). Arrows indicate GFP/GFAP double-positive cells. The percentage of GFAP-positive astrocytes in GFP-positive cells was quantified (B). Mean \pm S.D. The cells were also stained with antibodies against GFP (green) and β III-tubulin (red) (C). The percentage of β III-tubulin-positive neurons in GFP-positive cells was quantified (D). Mean \pm S.D. (E) E11.5 NPCs were infected with recombinant retroviruses engineered to express *EGFP* alone (pMYs), and *EGFP* together with either *N-myc* (N-myc) or *Hmga2* (Hmga2), and subsequently cultured for 4 days. GFP-positive cells were then sorted based on GFP fluorescence, and genomic DNA was extracted for bisulfite sequencing. White and black circles indicate unmethylated and methylated CpG sites, respectively. The E11.5 NPC sample was freshly prepared NPCs from telencephalon at E11.5. The CpG dinucleotide within the STAT3 binding site is indicated in red. (F) Methylation frequency in the *gfap* promoter. Mean \pm S.D. Scale bars = 50 μ m (A, C). For interpretation of the references to color in this figure legend, the reader is referred to the Web version of this article.

been reported to be expressed in a wide range of vertebrate tissues, primarily during embryogenesis (Schreiber-Agus et al., 1993). The mice deficient for functional *N-myc* are embryonic lethal (Stanton et al., 1992). Since *N-myc* has been shown to be a transcriptional activator, it may inhibit astrocyte differentiation via induction of neurogenic bHLH factors such as *Ngn1* (Sun et al., 2001), which have already been suggested to inhibit astrocyte differentiation in midgestational NPCs. However, this scenario seems unlikely because *N-myc* expression in NPCs did not affect neuronal differentiation, as assessed by monitoring expression of the neuronal marker β III-tubulin (Fig. 3C, D). On the other hand, *Hmga2* possesses an acidic C-terminal tail and three individual DNA-binding domains which bind short stretches of AT-rich DNA with high affinity (Reeves, 2001). *Hmga2* is expressed in pluripotent embryonic stem (ES) cells and in most tissues and organs during embryogenesis, but at very low levels or not at all in adult tissues (Zhou et al., 1995). Its function appears to be critical for cell growth, because mice lacking functional *Hmga2* exhibit a pygmy phenotype (Zhou et al., 1995). Recently, it was reported that *Hmga2* specifically accumulates on senescent cell chromatin and that it functions as a structural component of senescence-associated heterochromatin foci and as a repressor of proliferation-associated genes (Narita et al., 2006). We therefore expected that *Hmga2* would maintain the hypermethylation status of the astrocyte-specific *gfap* promoter via transcription-repressive heterochromatin formation in E11.5 NPCs. However, our results indicate that this is not the case. The mechanism(s) whereby *N-myc* and *Hmga2* inhibit astrocyte differentiation must await further investigation.

Although DNA methylation is a critical cell-intrinsic determinant for the neurogenic-to-astroglial switch and/or astrocyte differentiation of NPCs, many other spatio-temporally expressed extracellular factors such as CT-1, Notch and *Wnt1* (Barnabe-Heider et al., 2005; Hirabayashi and Gotoh, 2005; Nagao et al., 2007) and intracellular factors including *Ngn* (Sun et al., 2001), *N-CoR* (Hermanson et al., 2002), *N-myc* and *Hmga2* (this study) complement DNA methylation to ensure the sequential differentiation of NPCs during development. Thus, to better understand the mechanism underlying these processes, this study emphasizes the need to take cell-extrinsic cues, cell-intrinsic programs and factors, and their interaction into consideration.

Acknowledgments—We thank Dr. T. Kitamura (Tokyo University) for pMY vector and Plat-E cells. We appreciate Dr. Y. Bessho and T. Matsui for valuable discussions. We also thank Dr. I. Smith for helpful comments and critical reading of the manuscript. We are very grateful to N. Ueda for excellent secretarial assistance. Many thanks to N. Namihira for technical help. We also thank N. Moriyama for technical help with GeneChip analysis. This work has been supported by a Grant-in-Aid for Science Research on Priority Areas and the NAIST Global COE Program (Frontier Biosciences: Strategies for survival and adaptation in a changing global environment) from the Ministry of Education, Culture, Sports, Science and Technology (MEXT) of Japan.

REFERENCES

- Abramova N, Chamiga C, Goderie SK, Temple S (2005) Stage-specific changes in gene expression in acutely isolated mouse CNS progenitor cells. *Dev Biol* 283:269–281.
- Ajoka I, Maeda T, Nakajima K (2006) Identification of ventricular-side-enriched molecules regulated in a stage-dependent manner during cerebral cortical development. *Eur J Neurosci* 23:296–308.
- Alex R, Sozeri O, Meyer S, Dildrop R (1992) Determination of the DNA sequence recognized by the bHLH-zip domain of the N-Myc protein. *Nucleic Acids Res* 20:2257–2263.
- Barnabe-Heider F, Wasylanka JA, Fernandes KJ, Porsche C, Sendtner M, Kaplan DR, Miller FD (2005) Evidence that embryonic neurons regulate the onset of cortical gliogenesis via cardiotrophin-1. *Neuron* 48:253–265.
- Bonni A, Sun Y, Nadal-Vicens M, Bhatt A, Frank DA, Rozovsky I, Stahl N, Yancopoulos GD, Greenberg ME (1997) Regulation of gliogenesis in the central nervous system by the JAK-STAT signaling pathway. *Science* 278:477–483.
- Brunelli S, Innocenzi A, Cossu G (2003) *Bhlh5* is expressed in the CNS and sensory organs during mouse embryonic development. *Gene Expr Patterns* 3:755–759.
- Bugga L, Gadiant RA, Kwan K, Stewart CL, Patterson PH (1998) Analysis of neuronal and glial phenotypes in brains of mice deficient in leukemia inhibitory factor. *J Neurobiol* 36:509–524.
- Cai L, Morrow EM, Cepko CL (2000) Misexpression of basic helix-loop-helix genes in the murine cerebral cortex affects cell fate choices and neuronal survival. *Development* 127:3021–3030.
- Eklund T, Jessell TM (1999) Progression from extrinsic to intrinsic signaling in cell fate specification: a view from the nervous system. *Cell* 96:211–224.
- Graham V, Khudiyakov J, Ellis P, Pevny L (2003) SOX2 functions to maintain neural progenitor identity. *Neuron* 39:749–765.
- He F, Ga W, Martinowich K, Becker-Catania S, Coskun V, Zhu W, Wu H, Castro D, Guillemot F, Fan G, de Vellis J, Sun YE (2005) A positive autoregulatory loop of Jak-STAT signaling controls the onset of astroglial gliogenesis. *Nat Neurosci* 8:616–625.
- Hermanson O, Jepsen K, Rosenfeld MG (2002) N-CoR controls differentiation of neural stem cells into astrocytes. *Nature* 419: 934–939.
- Hirabayashi Y, Gotoh Y (2005) Stage-dependent fate determination of neural precursor cells in mouse forebrain. *Neurosci Res* 51: 331–336.
- Hsieh J, Gage FH (2004) Epigenetic control of neural stem cell fate. *Curr Opin Genet Dev* 14:461–469.
- Kanno J, Asaki K, Igarashi K, Nakatsu N, Ono A, Kodama Y, Nagao T (2006) “Per cell” normalization method for mRNA measurement by quantitative PCR and microarrays. *BMC Genomics* 7:64.
- Knoepfler PS, Cheng PF, Eisenman RN (2002) N-myc is essential during neurogenesis for the rapid expansion of progenitor cell populations and the inhibition of neuronal differentiation. *Genes Dev* 16:2699–2712.
- Koblar SA, Turnley AM, Classon BJ, Reid KL, Ware CB, Cheema SS, Murphy M, Bartlett PF (1998) Neural precursor differentiation into astrocytes requires signaling through the leukemia inhibitory factor receptor. *Proc Natl Acad Sci U S A* 95:3178–3181.
- Morita S, Kojima T, Kitamura T (2000) Plat-E: an efficient and stable system for transient packaging of retroviruses. *Gene Ther* 7: 1063–1066.
- Nagao M, Sugimori M, Nakafuku M (2007) Cross talk between notch and growth factor/cytokine signaling pathways in neural stem cells. *Mol Cell Biol* 27:3982–3994.
- Nakashima K, Wiese S, Yanagisawa M, Arakawa H, Kimura N, Hisatsune T, Yoshida K, Kishimoto T, Sendtner M, Taga T (1999a) Developmental requirement of gp130 signaling in neuronal survival and astrocyte differentiation. *J Neurosci* 19:5429–5434.
- Nakashima K, Yanagisawa M, Arakawa H, Kimura N, Hisatsune T, Kawabata M, Miyazono K, Taga T (1999b) Synergistic signaling in

- fetal brain by STAT3-Smad1 complex bridged by p300. *Science* 284:479–482.
- Narita M, Krizhanovsky V, Nunez S, Chicas A, Hearn SA, Myers MP, Lowe SW (2006) A novel role for high-mobility group proteins in cellular senescence and heterochromatin formation. *Cell* 126:503–514.
- Nieto M, Schuurmans C, Britz O, Guillemot F (2001) Neural bHLH genes control the neuronal versus glial fate decision in cortical progenitors. *Neuron* 29:401–413.
- Rajan P, McKay RD (1998) Multiple routes to astrocytic differentiation in the CNS. *J Neurosci* 18:3620–3629.
- Ramsay G, Stanton L, Schwab M, Bishop JM (1986) Human proto-oncogene N-myc encodes nuclear proteins that bind DNA. *Mol Cell Biol* 6:4450–4457.
- Reeves R (2001) Molecular biology of HMGA proteins: hubs of nuclear function. *Gene* 277:63–81.
- Saiki Y, Yamazaki Y, Yoshida M, Katoh O, Nakamura T (2000) Human EVB, a homologue of the mouse myeloid leukemia gene, is expressed in the hematopoietic progenitors and down-regulated during myeloid differentiation of HL60 cells. *Genomics* 70:387–391.
- Sawal S, Kato K, Wakamatsu Y, Kondoh H (1990) Organization and expression of the chicken N-myc gene. *Mol Cell Biol* 10:2017–2026.
- Schreiber-Agus N, Horner J, Torres R, Chiu FC, DePinho RA (1993) Zebra fish myc family and max genes: differential expression and oncogenic activity throughout vertebrate evolution. *Mol Cell Biol* 13:2765–2775.
- Sock E, Rettig SD, Enderich J, Bost MR, Tamm ER, Wegner M (2004) Gene targeting reveals a widespread role for the high-mobility-group transcription factor Sox11 in tissue remodeling. *Mol Cell Biol* 24:6635–6644.
- Stanton BR, Perkins AS, Tessarollo L, Sassoon DA, Parada LF (1992) Loss of N-myc function results in embryonic lethality and failure of the epithelial component of the embryo to develop. *Genes Dev* 6:2235–2247.
- Sun Y, Nadal-Vicens M, Misono S, Lin MZ, Zubiaga A, Hua X, Fan G, Greenberg ME (2001) Neurogenin promotes neurogenesis and inhibits glial differentiation by independent mechanisms. *Cell* 104:365–376.
- Takizawa T, Nakashima K, Namiura M, Ochiai W, Uemura A, Yanagisawa M, Fujita N, Nakao M, Taga T (2001) DNA methylation is a critical cell-intrinsic determinant of astrocyte differentiation in the fetal brain. *Dev Cell* 1:749–758.
- Temple S (2001) The development of neural stem cells. *Nature* 414:112–117.
- Tomita K, Moriyoshi K, Nakanishi S, Guillemot F, Kageyama R (2000) Mammalian achaete-scute and atonal homologs regulate neuronal versus glial fate determination in the central nervous system. *EMBO J* 19:5460–5472.
- Zhou X, Benson KF, Ashar HR, Chada K (1995) Mutation responsible for the mouse pygmy phenotype in the developmentally regulated factor HMGI-C. *Nature* 376:771–774.

(Accepted 13 June 2008)

(Available online 21 June 2008)

Integrative bioinformatics analysis of transcriptional regulatory programs in breast cancer cells

Atsushi Niida*¹, Andrew D Smith², Seiya Imoto³, Shuichi Tsutsumi⁴, Hiroyuki Aburatani⁴, Michael Q Zhang² and Tetsu Akiyama¹

Address: ¹Laboratory of Molecular and Genetic Information, Institute of Molecular and Cellular Biosciences, The University of Tokyo, 1-1-1, Yayoi, Bunkyo-ku, Tokyo, 110-0032, Japan, ²Cold Spring Harbor Laboratory, Cold Spring Harbor, NY 11724, USA, ³The Institute of Medical Science, The University of Tokyo, 4-6-1 Shirokanedai, Minato-ku, Tokyo 108-8639, Japan and ⁴Genome Science Division, Research Center for Advanced Science and Technology, The University of Tokyo, 4-6-1 Komaba, Meguro, Tokyo, 153-8904, Japan

Email: Atsushi Niida* - niida@iam.u-tokyo.ac.jp; Andrew D Smith - asmith@cshl.edu; Seiya Imoto - imoto@ims.u-tokyo.ac.jp; Shuichi Tsutsumi - shuichi@genome.rcast.u-tokyo.ac.jp; Hiroyuki Aburatani - haburata-ky@umin.ac.jp; Michael Q Zhang - mzhang@cshl.org; Tetsu Akiyama - akiyama@iam.u-tokyo.ac.jp

* Corresponding author

Published: 29 September 2008

Received: 17 January 2008

BMC Bioinformatics 2008, 9:404 doi:10.1186/1471-2105-9-404

Accepted: 29 September 2008

This article is available from: <http://www.biomedcentral.com/1471-2105/9/404>

© 2008 Niida et al; licensee BioMed Central Ltd.

This is an Open Access article distributed under the terms of the Creative Commons Attribution License (<http://creativecommons.org/licenses/by/2.0>), which permits unrestricted use, distribution, and reproduction in any medium, provided the original work is properly cited.

Abstract

Background: Microarray technology has unveiled transcriptomic differences among tumors of various phenotypes, and, especially, brought great progress in molecular understanding of phenotypic diversity of breast tumors. However, compared with the massive knowledge about the transcriptome, we have surprisingly little knowledge about regulatory mechanisms underlying transcriptomic diversity.

Results: To gain insights into the transcriptional programs that drive tumor progression, we integrated regulatory sequence data and expression profiles of breast cancer into a Bayesian Network, and searched for *cis*-regulatory motifs statistically associated with given histological grades and prognosis. Our analysis found that motifs bound by ELK1, E2F, NRF1 and NFY are potential regulatory motifs that positively correlate with malignant progression of breast cancer.

Conclusion: The results suggest that these 4 motifs are principal regulatory motifs driving malignant progression of breast cancer. Our method offers a more concise description about transcriptome diversity among breast tumors with different clinical phenotypes.

Background

Deregulation of transcriptional programs leads to development and progression of cancer, and many transcription factors (TFs) have been identified as oncogenes or tumor suppressor genes [1]. In the last decade, microarray technology has revolutionized cancer biology: microarray-based expression profiling studies have revealed that transcriptomes of cancer cells drastically change during carcinogenesis, and vary among different types of tumors.

Among many types of cancers, breast cancer has been attracting numerous investigators armed with microarray technology. Human breast tumors are diverse in their histology, prognosis, and responsiveness to treatments. Microarray technology has unveiled transcriptomic differences among tumors of various phenotypes, and brought great progress in molecular understanding of the phenotypic diversity. For example, Perou *et al.* [2] and Sorlie *et al.* [3] established that breast tumors are classified into

five different phenotypic subtypes. van't Veer *et al.* [4] and van de Vijver *et al.* [5] accurately divided breast cancer patients into two groups with favorable or unfavorable outcome, suggesting the potential of microarrays as a diagnostic test to select patients who would need adjuvant therapies. Many other studies have also identified gene signatures that enable us to predict distant metastasis or survival [6-8]. However, compared with the massive knowledge about the transcriptome, we have surprisingly little knowledge about regulatory mechanisms underlying transcriptomic diversity.

To analyze the transcriptional regulatory programs, computational approaches that integrate regulatory sequence data with global expression profiles are essential. So far, many approaches have been developed and successfully applied to lower organisms like yeast. For finding motifs that regulate gene expressions in yeast, linear regression-based methods use the correlation between the presence of cis-regulatory motifs and expression values [9,10]. A method employing multivariate adaptive regression spline (MARS) algorithm captured synergistic interactions between regulatory motifs and improved the prediction significantly as compared to that by the linear regression [11]. A method based on Bayesian networks also successfully identified combinational gene regulation by multiple motifs in yeast promoter sequences [12]. On the other hand, such challenges for gene regulation in higher eukaryotes like human are much harder owing to intrinsic complexity of their regulatory systems, and have just started [13,14]. As for breast cancer, although a small number of studies have also tried to decode transcriptional programs in cancer cell [15,16], it also remains to be tested whether transcriptional programs exist that are associated with, and potentially drive, breast tumor malignancy.

In this study, we propose a new approach to decipher transcriptional programs from cancer microarray data. Our method searches for the most probable motif combination associated with clinical phenotypes such as histological grade or survival time. Our approach has two major novel features. First, extending a previous work [12], we introduce a Bayesian scoring function which can treat continuous expression values. Secondly, instead of using raw expression values, we define a "meta-expression value" based on a correlation between gene expression profiles of a gene and a clinical phenotype, and then search for motifs correlated with meta-expression values. We show that application of our method to breast cancer microarray data successfully identified cis-regulatory motifs which are associated with malignancy of breast cancer.

Methods

Methods Overview

To elucidate transcriptional programs in cancer cells, we used a bioinformatics method based on Bayesian networks. We integrated regulatory sequences and global expression profiling data, and searched for cis-regulatory motifs statistically associated with clinical annotation accompanying the expression profiling data (Fig. 1).

We prepared three types of data to be integrated: regulatory sequences, regulatory motifs and expression profiling data. For regulatory sequences, we used core promoter sequences spanning 500 bp upstream and 100 bp downstream of the transcriptional start sites (TSSs). The regulatory motif data were prepared as position weight matrices (PWMs) by the following method: the known TF binding motifs were obtained from the TRANSFAC [17] and JASPAR database [18]. In addition, to complement missing information of the databases, we obtained potentially novel PWMs using an *ab initio* motif finder program, Discriminating Matrix Enumerator (DME, Smith *et al.*, 2005). Among similar types of motif finder programs, an exceptional feature of DME is that it identifies motifs based on relative over-representation between two sets of sequences. To obtain the *de novo* identified motif set, DME was applied to the regulatory sequences of gene groups which display highest and lowest expression values in expression value data. After reducing redundancy of these two PWM sets by clustering, the regulatory sequence of every gene was scored by each PWM. Then, the obtained scores are binarized using multiple thresholds to produce sequence features. Here, each sequence feature indicates the presence of a motif assuming one version of the multiple PWM thresholds. Prepared sequence features are collected to produce a sequence feature table. The sequence feature table is a binary matrix with its rows for genes and its columns for sequence features.

For expression value data, we prepared a publicly available data set of breast cancer expression profiles [7]. The data set includes expression values of 16,425 genes in 252 samples and information about a phenotype of each sample including its histological grades and patient prognosis. In our analyses, in stead of using the raw expression values, we used a "meta-expression value" calculated as a kind of correlation of the raw expression values with the phenotypes (e.g. differential expression between two sample groups of different histological grades or correlation with prognosis). Hence, the expression value matrix is transformed to a vector whose element is a meta-expression value of a gene. The expression value data were divided into training data and test data with a ratio of 3:1. Only information from the training data was used in a series of searches including *de novo* motif search using

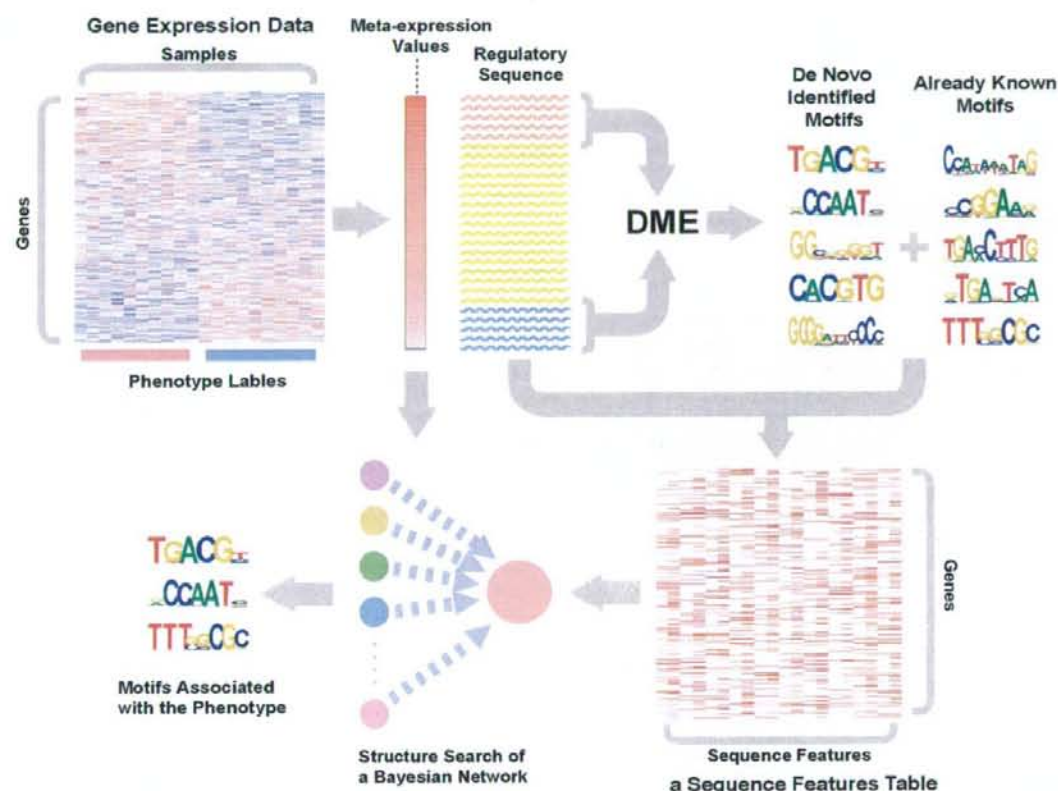


Figure 1

Schema of our method. We first calculate correlations between phenotypes and expression values as meta-expression values, while preparing a sequence feature table by searching promoter sequences for *cis*-regulatory motifs. *Cis*-regulatory motif data are prepared from two different sources: already known motifs, which are downloaded from databases, and *de novo* identified motifs, which were discovered by an *ab initio* motif finder program, DME. Then, associations between sequence features and meta-expression values were inferred by structure learning of Bayesian networks.

DME, and the test data were used for statistical evaluation of the result.

To infer associations between sequence features and the meta-expression values, our method learns parents of a single child node with methods originating from Bayesian network learning. We assumed a two-layer network structure where sequence features regulate the meta-expression values. In this case, the structural learning indicates that the method identifies the subset of sequence features that regulates the meta-expression values of each gene. This probabilistic approach is motivated by the work of Beer and Tavazoie [12], which successfully predicted gene expression patterns from combinations of regulatory

motifs in yeast. This approach can analyze nonlinear synergistic effects between regulatory motifs, which are thought to be more critical for gene regulation in higher eukaryotes. It can also incorporate flexible conditions of sequence features, such as the threshold value for PWM search. In the work of Beer and Tavazoie [12], the expression values were binarized to indicate whether each gene is assigned to an expression cluster. However, it is known that such discretization of data leads to loss of information [19]. Moreover, results yielded are potentially dependent on the threshold chosen in the discretization [20]. To solve this problem, our analysis introduces a new scoring function, which can deal with continuous meta-expression values. When a binary sequence feature table

and continuous meta-expression value data are given as the input data, the scoring function represents the posterior probability of a model that represents the dependency of the expression values and a combination of sequence features. By a greedy strategy, we searched for the most probable combination of sequence features so as to maximize the scoring function. Starting from the empty model, we iteratively added a sequence feature to the model as long as the value of the scoring function increases.

Regulatory sequence analysis

For regulatory sequence data, we prepared promoter data of 31,718 human genes from the Ensembl database (Release 40). Additionally, we also retrieved 27,967 mouse promoter sequences for comparative analysis (see below). Assuming the TSS as the start base of the gene assigned in Ensembl, a repeat-masked promoter sequence covering the 500 bp upstream and the 100 bp downstream of the TSS for each gene was extracted from the genome sequences.

For regulatory motif data, we prepared PWMs. The value f_{ib} of a PWM represents frequency of nucleotide base b at the i -th position in a motif. The frequencies of bases in each position are normalized so that $\sum_{b \in \{a, t, g, c\}} f_{ib} = 1$. If $f_{ib} = 0$, we assigned $f_{ib} = 0.001$ to avoid errors in log calculations. We acquired a total of 495 PWMs, which consist of vertebrate 367 PWMs annotated as "good" in TRANSFAC 10.1 [17], 123 PWMs from JASPAR core [18], and 5 PWMs from existing literature [21,22]. We then removed extremely simple or complex PWMs based on their information contents, and made a set of total 449 PWMs. Using the partition around medoids algorithm with the dissimilarity criterion based on the Kullback-Leibler divergence, the 449 PWMs are divided into 250 clusters (see Additional file 1). In the following analyses, we used 250 medoids of the clusters as the already known PWMs

In addition to the already known PWM set, we prepared motifs appearing frequently in promoter sequences of genes with high or low values in the expression value data. For the top 500 and the bottom 500 genes for expression values in the training data, we obtained their promoter sequences (the 500 bp upstream and the 100 bp downstream of the TSS) and those of their mouse homologs. We then searched for motifs relatively overrepresented in either set of sequences using the *ab initio* motif finder program, DME. For each identified PWM, its quality was evaluated based on classification error rate calculated by the MOTIFCLASS program in CREAD package. In accordance with the classification error rates, PWMs were ranked and clustered so as to reduce redundancy (see Additional file 1). We used the highest ranked PWM in each cluster and added them to the *de novo* identified PWM set.

To identify TF binding motifs in promoters, we used the log odds ratio L between a PWM and background base frequency f_b^{bg} . We calculated log odds ratio L_s for every subsequence of each promoter s (including the complementary strand), whose length is equal to the width of the motif of interest, w :

$$L_s = \sum_{i=1}^w \log \frac{f_i b_i}{f_b^{bg}}$$

In our analyses, f_b^{bg} is the base composition of each promoter, and the maximum of L_s in a human promoter sequence was taken as the motif score L^{human} for the sequence. For human genes whose mouse homologs are registered in Ensembl, L^{mouse} is also calculated. Then, L^{human} and L^{mouse} were averaged to produce the final score L . We found that this incorporation of homologous regulatory information improves our results, while PWM search combined with an ordinary phylogenetic footprinting approach reduces the performance presumably owing to the loss of sensitivity. For human genes that do not have any homologs, we used L^{human} as L . We assumed that the sequence has the motif if L is above the $p\%$ highest value in the population of all sequences. For all genes, we prepared binary data indicating the presence of the motif in their promoter with $p = 5, 10, 15$, and 20. This procedure was iterated for all members of the *de novo* identified and already known PWM set to produce the sequence feature table.

Expression data analysis

Expression data [7] produced by Affymetrix GeneChips were downloaded from the Gene Expression Omnibus (GEO) database at NCBI (The GEO accession number is GSE3494). Absolute expression values of a data set were converted to the log scale and normalized so that the mean is equal to 0 and the variance is equal to 1 in each sample. The probe set IDs were converted to Ensembl gene IDs. In cases that one gene ID matches multiple probe set IDs, the probe set which shows the most variance among the samples was mapped to the gene. For in total 16,425 genes, we prepared meta-expression values for subsequent Bayesian network analysis by calculating differential expression between two sample groups or correlation with survival time as described below. The meta-expression values were also normalized so that the mean is equal to 0 and the variance is equal to 1.

Since the samples are separated into two groups, we measured differential expression of each gene between the two

groups based on t-statistic. To evaluate the significance of differential expression, a null distribution of the t-statistic was produced from 100 data sets with randomly permuted sample labels. Based on the null distribution, the P-value was computed by two-sided test. To correct multiple hypotheses testing, the P-values were converted to Q-values using the qvalue package of R [23].

For Survival time information, we measured univariate correlation of each gene with survival time using the Cox proportional hazards regression method [24], we used the ratio of each regression coefficient to its standard error as the correlation value with poor prognosis.

Bayesian network analysis

For selecting the network structure N of the Bayesian network, we apply a Bayesian approach. According to Bayes' theorem, the posterior probability of the network structure, $p(N|D)$, is proportional to the product of the prior probability of the network structure, $p(N)$ and the likelihood $p(D|N)$ as

$$p(N|D) = \frac{p(N)p(D|N)}{p(D)} \propto p(N)p(D|N).$$

Based on this formula, we can infer the network structure N hidden behind the data D . In our analyses, we assumed that a network structure N is composed of a single child node and multiple parent nodes. The single child node has a continuous variable x representing a meta-expression value, and parent nodes have binary variables indicating the presence or absence of sequence features. The data D is composed of M meta-expression values and their sequence feature information. For a given data D , we search parent nodes, i.e., sequence features, for each group of meta-expressions by maximizing $p(N|D)$.

The likelihood

Suppose that we have gene expression profiles of M genes measured by a number of microarrays. The meta-expression vector, x , is then computed as the M -dimensional vector whose the i th element, x_i , represents the meta-expression value of the i th gene. We also assume that S is the sequence feature table whose the (i, j) th element, s_{ij} , takes one if the i th gene has the j th sequence feature in its promoter region, or zero otherwise. The network structure, N , specifies the set of sequence features as the parents of the meta-expression values. For example, if N specifies the two parents for the meta expression values, we then consider a three nodes Bayesian network with observations $\{(x_i, s_{q_1}, s_{q_2}) : i = 1, \dots, M\}$, where $j_1, j_2 \in \{1, \dots, n\}$ and $j_1 \neq j_2$. Here n is the number of columns in S , i.e., the

number of sequence features of interest. Our structural learning of Bayesian networks is to find the optimal combination of sequence features as the parents of meta-expression values.

In the problem stated above, we would like to discuss our model for meta-expressions when the networks structure is given. Since the information of sequence features take binary variables, i.e., 0 or 1, the parent variables can theoretically take 2^{n_p} patterns, where n_p is the number of parents specified by the network structure. In the above example, the network model chooses two motifs as the parents and there are four patterns, $\{(0, 0), (0, 1), (1, 0), (1, 1)\}$, that the parents can take. In practice, since it is a possible case that we cannot find all the patterns of specified parents in S for large n_p , we denote the number of observed patterns by q ($q \leq 2^{n_p}$). Therefore, if we specified the network structure, the meta-expression values can be separated into q exclusive groups. That is, the parents of the meta-expressions in each group show the same pattern.

More mathematically, let $s_i = \{s_{i1}, \dots, s_{in}\}$ be the i th row of S . Based on the specified structure N , we define the subset $s_i(N) = \{s_{i,p_1}, \dots, s_{i,p_r}\}$ as the parents of meta-expressions, where $\{p_1, \dots, p_r\} \subset \{1, \dots, n\}$. We then have the following decomposition:

$$\begin{aligned} p(D|N) &= \prod_{i=1}^M p(x_i, s_i | N) \\ &= \prod_{i=1}^M p(x_i | s_i, N) p(s_i | N) \\ &\propto \prod_{i=1}^M p(x_i | s_i(N)) \\ &= \prod_{k=1}^q p(d_k | pa_k), \end{aligned}$$

where pa_k is the k th pattern of parent motifs and d_k is the set of meta-expressions that have the same sequence feature information restricted by the parent motifs. For example, if $s_1(N)$ and $s_2(N)$ are equal to pa_1 , then x_1 and x_2 are included in d_1 . Note that we assume $p(s_i|N) = p(s_i)$ follows uniform distribution and is independent from the selection of network structure N .

We next consider a statistical model for $p(d_k|pa_k)$. By omitting the subscript k and the parent state, we denote $p(d_k|pa_k)$ as $p(d)$. Suppose that M_k meta-expression values are included in the group, i.e., $d = \{x^{(1)}, \dots, x^{(M_k)}\}$. Note that we also denote M_k as M hereafter. We fit a normal distribution to each element of d by

$$\phi(x^{(m)} | \mu, \tau) = \sqrt{\frac{\tau}{2\pi}} \exp\left\{-\frac{\tau(x^{(m)} - \mu)^2}{2}\right\}, \quad m = 1, \dots, M,$$

where $\phi(x|\mu, \tau)$ is the density of normal distribution with mean μ and variance τ^{-1} . Note that τ is called precision. We assume that the joint prior density of mean and precision, μ and τ , is decomposed by

$$p(\mu, \tau) = p(\mu|\tau)p(\tau).$$

The conditional density of μ is set as

$$p(\mu | \tau) = \phi(\mu | \mu_0, \lambda_0 \tau) = \sqrt{\frac{\lambda_0 \tau}{2\pi}} \exp\left\{-\frac{\lambda_0 \tau (\mu - \mu_0)^2}{2}\right\},$$

where μ_0 and λ_0 are hyperparameters. The marginal distribution of the precision, τ , is set by the density of gamma distribution with hyperparameters, α_0 and β_0 , and given by

$$p(\tau) = g(\tau | \alpha_0, \beta_0) = \frac{\beta_0^{\alpha_0}}{\Gamma(\alpha_0)} \tau^{\alpha_0-1} \exp(-\beta_0 \tau).$$

In this setting, $p(\mu, \tau)$ is the density of normal-gamma distribution with hyperparameters, $\mu_0, \lambda_0, \alpha_0$ and β_0 . Hence, the marginal likelihood $p(d)$ is given by

$$\begin{aligned} p(d) &= \int_{\tau=0}^{\infty} \int_{\mu=-\infty}^{\infty} p(d | \mu, \tau) p(\mu, \tau) d\mu d\tau \\ &= \int_{\tau=0}^{\infty} \int_{\mu=-\infty}^{\infty} \left\{ \prod_{m=1}^M \phi(x^{(m)} | \mu, \tau) \right\} \phi(\mu | \mu_0, \lambda_0 \tau) g(\tau | \alpha_0, \beta_0) d\mu d\tau. \end{aligned}$$

Since the normal-gamma distribution is a conjugate prior of normal distribution model, the integral in the marginal likelihood can analytically be calculated. Hence, by putting

$$\begin{aligned} \bar{x} &= \frac{1}{M} \sum_{m=1}^M x^{(m)}, \\ \lambda_1 &= \lambda_0 + M, \\ \mu_1 &= \frac{\lambda_0 \mu_0 + M \bar{x}}{\lambda_1}, \\ \alpha_1 &= \alpha_0 + \frac{M}{2}, \\ \beta_1 &= \beta_0 + \frac{1}{2} \sum_{m=1}^M (x^{(m)} - \bar{x})^2 + \frac{M \lambda_0 (\bar{x} - \mu_0)^2}{2 \lambda_1}, \end{aligned}$$

we then have

$$p(d) = \frac{1}{(2\pi)^{M/2}} \cdot \frac{\Gamma(\alpha_1)}{\Gamma(\alpha_0)} \cdot \frac{\beta_0^{\alpha_0}}{\beta_1^{\alpha_1}} \cdot \left(\frac{\lambda_0}{\lambda_1}\right)^{1/2}.$$

The details of this calculation are shown in Additional file 1. Hence, the marginal likelihood, $p(D|N)$, is obtained as the function of the hyperparameters $\{\mu_{0j}, \lambda_{0j}, \alpha_{0j}, \beta_{0j}\}$ and is given by

$$p(D | N) = \prod_{k=1}^g \frac{1}{(2\pi)^{M_k/2}} \cdot \frac{\Gamma(\alpha_{1k})}{\Gamma(\alpha_{0k})} \cdot \frac{\beta_{0k}^{\alpha_{0k}}}{\beta_{1k}^{\alpha_{1k}}} \cdot \left(\frac{\lambda_{0k}}{\lambda_{1k}}\right)^{1/2}.$$

In our analysis, we set $\mu_{0k} = 0, \lambda_{0k} = 10, \alpha_{0k} = 9/2$ and $\beta_{0k} = 10/2$ for all k .

The prior probability

To avoid overfitting to the training data, the prior probability of the network $p(N)$ was specified so as to penalize complex networks:

$$p(N) = cK^{-n_p},$$

where c is a constant that makes $\sum p(N) = 1, K$ is a parameter that specifies how strongly complexity is penalized, and n_p is the number of parent nodes in the network. As K decreases, the networks grow larger, and the number of parent nodes increases. Initially this increase in complexity reflects actual combinatorial regulation. However, after exceeding a point, false positive increase gradually owing to overfitting to the training data. To optimize the value of K , we performed preliminary runs with $K = 10, 15, 20, 25, 30$. We checked P-values for the training data, and chose $K = 20$ because it allows sufficient sensitivity and a minimum of false positives.

Search algorithm

To search for the most probable parent nodes based on the scoring function $p(N)p(D|N)$, we took greedy search strategy. We started from structure without any edge

between the child node and the parent node candidates and iteratively added an edge from a parent node candidate. For each iterative cycle, we calculated the score of $p(N)p(D|N)$ for every case where the edge from the each parent node candidate was added, and the maximizer of them was added to the structure. The cycle repeated until no more edge increases the score. To speed up the search, we utilized clustering of parent node candidates (see Additional file 1).

Results

Transcriptional programs correlating with histological grades

Focusing on transcriptional regulatory programs that control histological diversity, we searched for *cis*-regulatory motifs associated with histological grades. Histological grading in breast cancer seeks to integrate measurements of cellular differentiation and replicative potential into a composite score that quantifies the aggressive behavior of a tumor. The most studied and widely used method is the Elston-Ellis modified Scarff, Bloom, Richardson grading system, also known as the Nottingham Grading System [25]. The Nottingham Grading System is based on a microscopic evaluation of morphologic and cytologic features of tumor cells, including degree of tubule formation, nuclear pleomorphism, and mitotic count. The sum of these scores stratifies breast tumors into grade 1 (G1; well-differentiated), grade 2 (G2; moderately differentiated), and grade 3 (G3; poorly differentiated, highly proliferative) malignancies. It has been well known that the grade of breast cancer is a powerful indicator of disease recurrence and patient death. Untreated patients with G1 disease have a ~95% 5-year survival rate whereas those with G2 and G3 malignancy have survival rates at 5 years of ~75% and ~50%, respectively. Comparison between global expression profiles of tumor cells of different grades also revealed distinct expression patterns, especially between G1 and G3 groups [26].

For each gene in the global expression profile data, we calculated the degree of differential expression between two sample groups (67 G1 and 54 G3 samples). We then applied our method to the differential expression value to search for correlating motifs. The results were evaluated in two ways. First, reproducibility of the result was assessed by bootstrap analysis. Structure learning of a Bayesian network was repeated 30 times using bootstrap samples from the training dataset. We found that V\$ELK1_02, V\$E2F1_Q4_01, V\$NRF1_Q6 and JSP\$NF_Y were reproducibly selected by the bootstrap analysis (Figure 2). Here, IDs starting from "V\$", "JSP\$" and "DME\$" motifs denote motifs from the TRANSFAC database, the JASPAR database and our DME analysis, respectively. For V\$ELK1_02, highly similar motifs sampled by DME also reproducibly appeared. Although we present here results

based on one training-test set partition, for checking robustness of biological findings, we applied our method to different training-test set partitions. We confirmed that almost the same results were obtained with different training-test set partitions. Secondly, statistical significance was evaluated for each of the sequence features reproducibly selected by the bootstrap analysis. We assessed difference of expression values between two gene groups with and without each sequence feature, using Wilcoxon rank sum test for the training and test data. It should be noted that, because the P-values calculated using the training data is not subject to multiple testing corrections, it can potentially achieve low values by overfitting to the training data. Hence, we must use the P-values calculated using the test data to accurately evaluate statistical significance. The results from the Wilcoxon rank sum tests suggest that sequence features that are most significantly associated with the histological grades are V\$ELK1_02(20) V\$E2F1_Q4_01(10), V\$NRF1_Q6(10) and JSP\$NF_Y(10) (The IDs are followed by values of the threshold parameter for motif searches in parentheses). P-values were also calculated for these four sequence features as a combination. We split genes into 16 groups based on combinations of the presence and absence of the 4 sequence feature, and evaluated difference of expression value distributions among the gene groups using Kruskal-Wallis test. Our calculation shows that the combination of these four sequence features scores highly significant a P-value of 1.33×10^{-15} for the test data. Analyses using independent data sets and prediction based on the MAP-value also confirmed these results (see Additional file 1).

We next investigated how differential expression between G1 and G3 tumors depends on these four sequence features. We divided genes into 16 groups based on patterns of these four sequence features, and differences in distribution of their expression values were examined (see Supplementary Table 1 in Additional file 1). The box plots in Figure 3 summarize the results. For clarity, gene groups of similar distributions were gathered to form one group. These results indicate that these sequence features are additively associated with upregulation of gene expression in G3 populations.

Transcriptional programs correlating with prognosis

We also examined regulatory programs associated with prognosis, a more direct measure of tumor malignancy. For each gene, correlation values with survival time were calculated using Cox regression models [24]. Then, we searched for *cis*-regulatory motifs associated with the correlation values using our method. Our analysis selected V\$ELK1_02(10), V\$E2F1_Q4_01(5), V\$NRF1_Q6(15) and JSP\$NF_Y(10) as sequence features positively associated with prognosis, similarly to the analysis for histological grade (Figure 4, Supplementary Table 2 in Additional

^a Motif ID	Logo	^b Reproducibility	^c P value for training data	^d P value for test data
^f V\$ELK1_02(20)		23	3.44x10 ⁻²⁸	8.97x10 ⁻¹⁰
^g JSP\$NF_Y(10)		16	9.17x10 ⁻¹⁰	0.000193
^h V\$NRF1_Q6(10)		11	1.28x10 ⁻¹⁸	8.00x10 ⁻¹⁰
DME\$TTYRAAYYN(10)		11	0.00134	0.977
DME\$WYTSAAAYNNN(5)		7	4.96x10 ⁻⁵	0.696
JSP\$NF_Y(20)		7	1.17x10 ⁻⁹	0.0015
V\$NRF1_Q6(20)		7	1.10x10 ⁻²²	7.50x10 ⁻⁸
ⁱ V\$E2F1_Q4_01(20)		7	3.37x10 ⁻¹⁵	7.76x10 ⁻⁸
^e DME\$RMNSCGGAASY(5)		7	4.24x10 ⁻⁷	0.000841
V\$E2F1_Q4_01(10)		7	1.16x10 ⁻¹³	9.54x10 ⁻¹⁰

^a IDs starting from "V\$", "JSP\$", and "DME\$" Motifs denote motifs from the TRANSFAC database, the JASPAR database, and our DME analysis, respectively, followed by values of the threshold parameter for motif searches in parentheses.

^b The number of appearances of sequence feature in 30 searches with bootstrap resampling.

^{c,d} P values calculated by Wilcoxon rank sum tests for training and test data, respectively.

^e Highly similar to V\$ELK1_02.

^{f,g,h,i} For these four sequence features, P values were calculated as 1.37×10^{-43} and 1.33×10^{-15} by Kruskal-Wallis test for the training data and the test data, respectively.

Figure 2
Sequence features associated with differential expression between G1 and G3 breast tumors.

file 1, and Figure 5). A P-value for a combination of these four motifs was calculated as 7.17×10^{-12} for the test data.

Robustness of our biological findings

To confirm robustness of our biological findings, we analyze independent data published by Sotiriou *et al.*

[27](189 samples × 12466 genes) and Pawitan *et al.* [28](159 samples × 16425 genes). Similar to the results obtained in the above analyses, we found that the binding motifs of E2F, ELK1, NRF1 and NFY show significant correlation of histological grades and prognosis (Table 1), indicating the robustness of our findings. Taken together,

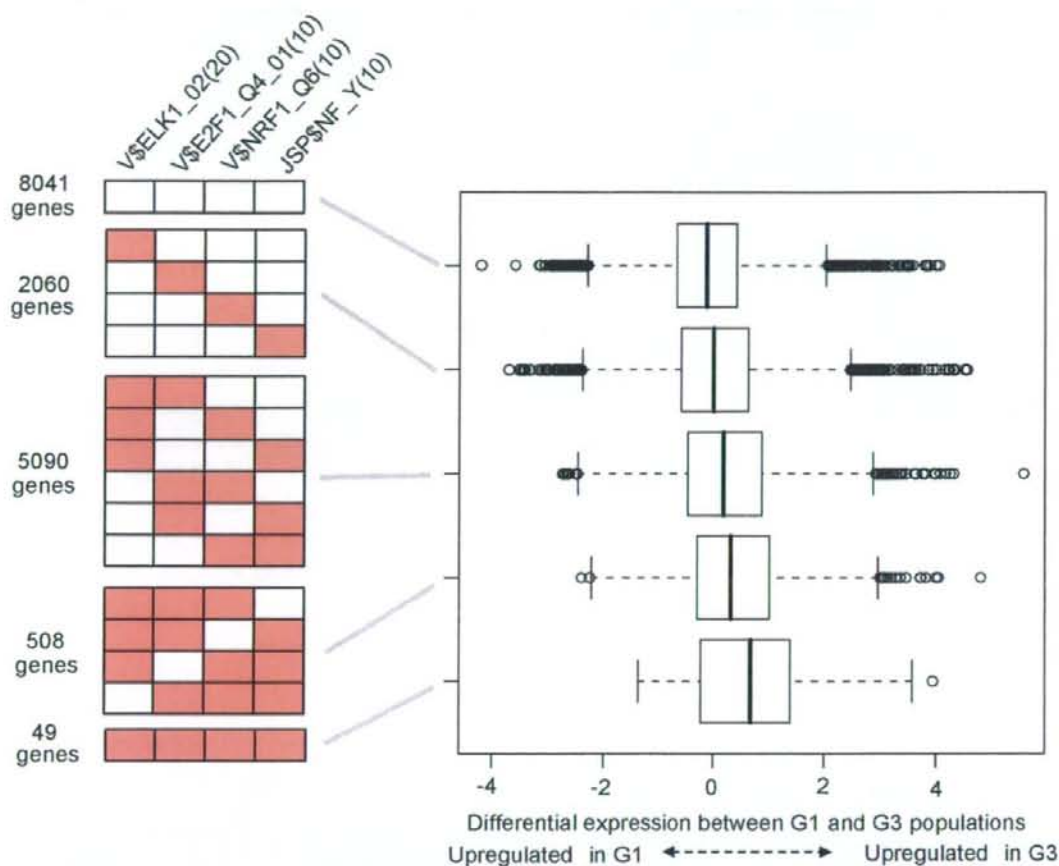


Figure 3
Dependency of differential expression between G1 and G3 breast tumors on sequence features. Genes are divided into five groups based on patterns of four sequence features, V\$ELK1_Q2(20), V\$E2F1_Q4_Q1(10), V\$NRF1_Q6(10) and JSP\$NF_Y(10) (the left red boxes indicates the presence of sequence features). The distributions of their differential expression values between G1 and G3 are displayed using box plots.

we conclude that *cis*-regulatory motifs bound by these 4 TFs are principal motifs associated with breast cancer malignancy.

Discussion

To decode transcriptional program in breast cancer, we developed a novel approach employing a new Bayesian scoring function and meta-expression value. Combining promoter sequence and expression data, we searched for *cis*-regulatory motifs correlated with histological grade and prognosis.

As motif sets to be searched, we prepared known motifs from databases, and *de novo* motifs identified by a motif discovery program, DME. As motifs correlated with malignancy, we identified the ELK1 binding motif as well as a highly similar *de novo* one, demonstrating success in our approach. Judging from statistical evaluations, the known motif shows better performance than the *de novo* one. Further improvement of the motif finder program will enable us to identify *de novo* motifs of higher quality. Our method introduced a new Bayesian approach, which can deal with multiple sequence features and a continuous

Table 1: Motif associated with histological grades or prognosis identified based on independent datasets

	^a Motif ID	^b Reproducibility	^c P value for training data	^d P value for test data
motifs associated with histological grades based on the data by Sotiriou et al.	JSP\$NF_Y(20)	20	3.1×10^{-10}	0.000158
	V\$NRFI_Q6(10)	15	3.09×10^{-14}	6.02×10^{-7}
	V\$ELK1_Q2(20)	12	9.25×10^{-24}	1.41×10^{-4}
	DME\$CTTCCGSYN(5)	9	5.71×10^{-14}	6.82×10^{-5}
	V\$E2FI_Q4_01(5)	7	5.71×10^{-15}	0.002372
motifs associated with prognosis based on the data by Sotiriou et al.	JSP\$NF_Y(10)	15	2.46×10^{-14}	0.011049
	DME\$RMSYSSARGCGC(5)	11	4.02×10^{-5}	0.063412
	V\$ELK1_Q2(10)	10	2.03×10^{-16}	2.08×10^{-7}
	DME\$YYYGSGCMYGC(5)	8	1.65×10^{-9}	0.008054
	V\$E2FI_Q4_01(10)	8	1.05×10^{-17}	2.37×10^{-5}
	V\$IRF_Q6_01(10)	7	2.06×10^{-8}	0.000152
	DME\$NMSTTCYKSYR(5)	6	0.000669	0.084446
V\$NRFI_Q6(20)	6	9.02×10^{-22}	1.31×10^{-4}	
motifs associated with histological grades based on the data by Pawitan et al.	JSP\$NF_Y(20)	22	5.93×10^{-8}	0.01116
	V\$E2FI_Q4_01(5)	10	6.56×10^{-7}	0.049423
	DME\$RCRKGCGCAVN(5)	6	5.71×10^{-8}	0.060899
	V\$E2FI_Q4_01(15)	6	9.59×10^{-6}	0.017285
motifs associated with prognosis based on the data by Pawitan et al.	V\$ELK1_Q2(20)	16	1.26×10^{-27}	6.13×10^{-12}
	V\$NRFI_Q6(15)	11	9.2×10^{-23}	3.89×10^{-7}
	V\$NRFI_Q6(20)	11	4.31×10^{-22}	2.49×10^{-7}
	V\$ELK1_Q2(15)	9	1.63×10^{-25}	6.41×10^{-11}
	DME\$RCGCHKGCGY(5)	6	3.23×10^{-20}	4.8×10^{-6}

^aIDs starting from "V\$", "JSP\$", and "DME\$" Motifs denote motifs from the TRANSFAC database, the JASPAR database, and our DME analysis, respectively, followed by values of the threshold parameter for motif searches in parentheses.







^bThe number of appearances of sequence feature in 30 searches with bootstrap resampling.

^{c,d}P values calculated by Wilcoxon rank sum tests for training and test data, respectively.

meta-expression value. Compared to previous methods, our method more efficiently analyzes motif combination without thresholding meta-expression values (see Additional file 1). It should be noted that found motif combinations are no guarantee of a true synergistic, cooperative interaction of the related TFs; further studies remain to be done for analysis of motif interactions. Utilization of meta-expression values is also a novel feature of our method. Although we focused on histological grade and prognosis of breast cancer in this study, our approach can easily be extended to analyze other pathologies and other clinical variables. In addition to these features, we found that our method is robust on the data complexity; we found that our method leads to essentially the same result for grade-associated motifs even if we use only half of the patient data (see Supplementary Table 6 in Additional file 1).

Our analysis identified *cis*-regulatory motifs bound by ELK1, E2F1, NRF1 and NFY as principal motifs associated

with breast cancer malignancy. ELK1 is a member of the ETS transcription factor family. Because the ETS family of transcription factors binds to similar motifs with a central core sequence GGA(A/T), ELK1 binding motifs are potentially bounded by other ETS family members. It has been reported that many of them are downstream nuclear targets of Ras-MAP kinase signaling, and the deregulation of the ETS genes results in malignant transformation and tumor progression. Several ETS genes are rearranged in human leukemia and Ewing tumor to generate chimeric oncoproteins. Furthermore, the aberrant expression of several ETS genes is often observed in various types of human malignant tumors [29]. Many of the ETS family transcription factors are upregulated in the G3 population: ETV7 ($Q = 7.79 \times 10^{-5}$), ELF4 ($Q = 0.00182$), ELF5 ($Q = 0.0270$), GABPA ($Q = 0.0301$), SPIB ($Q = 0.0344$), ELF3 ($Q = 0.0383$), ETV4 ($Q = 0.0386$) and ETS1 ($Q = 0.0468$). A recent study based on integrative bioinformatics also suggests that a ETS-directed transcriptional program is involved in malignant progression of prostate

^a Motif ID	Logo	^b Reproducibility	^c P value for training data	^d P value for test data
^f V\$NRF1_Q6(15)		21	4.47x10 ⁻²⁵	3.93x10 ⁻⁶
^g V\$ELK1_02(10)		14	1.68x10 ⁻²⁶	3.54x10 ⁻⁸
^e DME\$RCTTCCGSN(5)		13	4.04x10 ⁻²⁵	0.0001
^h V\$E2F1_Q4_01(5)		9	4.19x10 ⁻¹⁶	0.000338
ⁱ V\$NRF1_Q6(20)		9	3.13x10 ⁻²⁰	2.99x10 ⁻⁶
JSP\$NF_Y(10)		8	1.86x10 ⁻¹³	0.00042

^a IDs starting from "V\$", "JSP\$", and "DME\$" Motifs denote motifs from the TRANSFAC database, the JASPAR database, and our DME analysis, respectively, followed by values of the threshold parameter for motif searches in parentheses

^b The number of appearances of sequence feature in 30 searches with bootstrap resampling

^{c,d} P values calculated by Wilcoxon rank sum tests for training and test data, respectively

^e Highly similar to V\$ELK1_02.

^{f,g,h,i} For these four sequence features, P values were calculated as 4.63x10⁻⁵³ and 7.17x10⁻¹² by Kruskal-Wallis test for the training data and the test data, respectively.

Figure 4
Sequence features associated with the correlation value calculated for breast cancer prognosis.

cancer [30]. Further integrative studies are required to examine whether ETS-directed transcriptional programs contributes to malignancy in various types of tumors.

The E2F family includes transcription factors which form heterodimer complexes with DP proteins and recognize a common motif [31]. The E2F family of proteins is known to be a master regulator of the cell cycle. The association of the E2F motif with G3 is therefore consistent with the fact that the histological grading criteria include the mitotic index and that G3 tumors are defined as highly proliferative. We also observed that most of the E2F family members and two DP genes are significantly upregulated in G3 tumors: E2F8 (Q < 10⁻⁶), E2F3 (Q < 10⁻⁶), E2F1 (Q < 10⁻⁶), E2F6 (Q = 3.14 × 10⁻⁵), E2F5 (Q = 0.0219), DP2 (Q = 0.00167) and DP1 (Q = 0.0111).

NRF1 has been reported to induce nuclear-encoded mitochondrial genes and increase mitochondrial respiratory

capacity [32]. Though no clear function of NRF1 in cancer cells has been reported, our finding that the NRF1-binding motif correlates with tumor malignancy may reflect hypermetabolism in aggressive tumors. It has also been reported that NRF1 collaborates with E2F family members to regulate genes involved in cellular proliferations [33].

The NFY-binding motif, the CCAAT box, is one of the first identified and most common elements in eukaryotic promoters. On the other hand, elucidation of regulatory networks involving NFY motifs has been hampered by their generality. Our result raises the possibility that NFY-binding motif functions malignant breast cancers cooperatively with other factors. In fact, a previous study reported that NFY and E2F functionally interact to regulate cell cycle genes [34].

Although we successfully identified above regulatory motifs, we failed to identify the motifs bounded by tran-

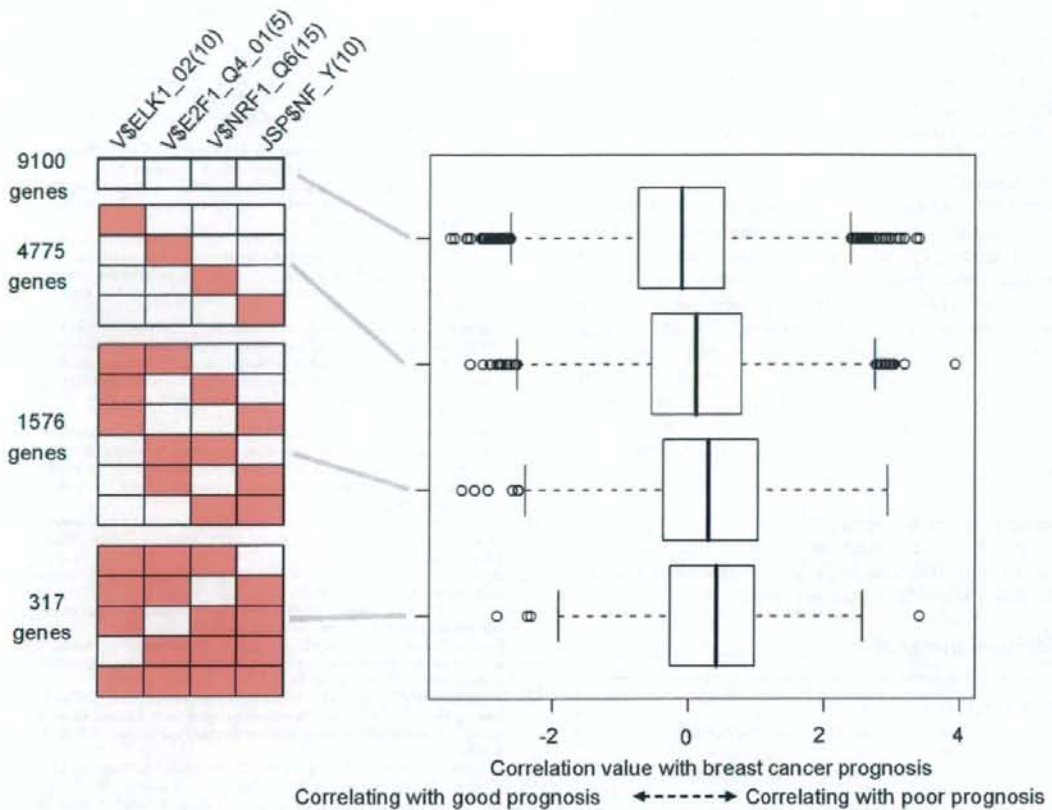


Figure 5
Dependency of the correlation value with breast cancer prognosis on sequence features. Genes are divided into five groups based on patterns of four sequence features, V\$ELK1_Q2(5), V\$E2F1_Q4_Q1(10), V\$NRF1_Q6(15) and JSP\$NF_Y(10) (the left red boxes indicates the presence of sequence features). The distributions of their correlation value with breast cancer prognosis are displayed using box plots.

scription factors that are thought to be more critically associated with breast cancer malignancy, including the estrogen receptor and p53. One reason for this failure is that, since the number of target genes varies between transcriptional regulators, our method "skims off" only strong signals from motifs bound by regulators having a sufficient number of target genes. However, a more likely reason is that our method focuses on only proximal regulatory sequences. Each TFs has a positional preference: some TFs bind mainly proximal promoters around the TSSs while others can act on distal enhancer sequences. Recent comprehensive ChIP analyses have clearly shown that the estrogen receptor and p53 have a

broad range of positional preference [35,36]. Computational predictions [22] and genome-wide experiments [37,38] have just started to produce distal regulatory sequence data; incorporation of such information will solve this problem.

In cancer cells, genetic and epigenetic alterations also have great impact on gene expression at the mRNA level. Currently, comprehensive data of genomic copy number [39] and epigenetic status [40] are also accumulating. One of the next important challenges will be to incorporate them and decompose gene expression signals from different molecular mechanisms.

Considering the exploding availability of genome-wide experimental data, we can be optimistic that the integrative bioinformatics approach will circumvent these limitations in the near future. Future work will focus on further refinement of our approach toward a deeper understanding of transcriptional programs in cancer cells.

Conclusion

In this study, we introduced a new approach to analyze cancer microarray data. While many studies have focused on correlation between gene expression and a clinical phenotype, our method associates *cis*-regulatory motifs with clinical phenotypes. This approach offers a more concise description of transcriptome diversity among samples with different clinical phenotypes. Using this method, we demonstrated that *cis*-regulatory motifs bound by ELK1, E2F, NRF1 and NFY are most significantly associated with breast cancer malignancy. Our data suggest that they are principal regulatory motifs driving breast cancer malignant progression.

Authors' contributions

AN, TA, ST, and HA designed research; AN performed research; AN, ADS and MQZ contributed new analytic tools; AN, TA, and SI wrote the paper.

Additional material

Additional file 1

supplementary methods, discussions, tables and figures.

Click here for file

[http://www.biomedcentral.com/content/supplementary/1471-2105-9-404-S1.pdf]

Acknowledgements

Computation time was provided by the Super Computer System, Human Genome Center, Institute of Medical Science, University of Tokyo. This work was supported by Grants-in-Aid for Scientific Research on Priority Areas. A. N. was supported by Research Fellowships from Japan Society for the Promotion of Science for Young Scientists.

References

- Darnell JE Jr: **Transcription factors as targets for cancer therapy.** *Nat Rev Cancer* 2002, **2**:740-749.
- Perou CM, Sorlie T, Eisen MB, Rijn M van de, Jeffrey SS, Rees CA, Pollack JR, Ross DT, Johnsen H, Akslen LA, Fluge O, Pergamenschikov A, Williams C, Zhu SX, Lonning PE, Borresen-Dale AL, Brown PO, Botstein D: **Molecular portraits of human breast tumours.** *Nature* 2000, **406**:747-752.
- Sorlie T, Perou CM, Tibshirani R, Aas T, Geister S, Johnsen H, Hastie T, Eisen MB, Rijn M van de, Jeffrey SS, Thorsen T, Quist H, Matese JC, Brown PO, Botstein D, Eystein Lonning P, Borresen-Dale AL: **Gene expression patterns of breast carcinomas distinguish tumor subclasses with clinical implications.** *Proc Natl Acad Sci USA* 2001, **98**:10869-10874.
- van't Veer LJ, Dai H, Vijver MJ van de, He YD, Hart AA, Mao M, Peterse HL, Kooy K van der, Marton MJ, Witteveen AT, Schreiber GJ, Kerkhoven RM, Roberts C, Linsley PS, Bernards R, Friend SH: **Gene expression profiling predicts clinical outcome of breast cancer.** *Nature* 2002, **415**:530-536.
- Vijver MJ van de, He YD, van't Veer LJ, Dai H, Hart AA, Voskuil DW, Schreiber GJ, Peterse JL, Roberts C, Marton MJ, Parrish M, Atsma D, Witteveen A, Glas A, Delahaye L, Velde T van der, Bartelink H, Rodenhuis S, Rutgers ET, Friend SH, Bernards R: **A gene-expression signature as a predictor of survival in breast cancer.** *N Engl J Med* 2002, **347**:1999-2009.
- Wang Y, Klijn JG, Zhang Y, Sieuwerts AM, Look MP, Yang F, Talantov D, Timmermans M, Meijer-van Gelder ME, Yu J, Jatkoe T, Berns EM, Atkins D, Foekens JA: **Gene-expression profiles to predict distant metastasis of lymph-node-negative primary breast cancer.** *Lancet* 2005, **365**:671-679.
- Miller LD, Smeds J, George J, Vega VB, Vergara L, Ploner A, Pawitan Y, Hall P, Klaar S, Liu ET, Bergh J: **An expression signature for p53 status in human breast cancer predicts mutation status, transcriptional effects, and patient survival.** *Proc Natl Acad Sci USA* 2005, **102**:13550-13555.
- Chang HY, Nuyten DS, Sneddon JB, Hastie T, Tibshirani R, Sorlie T, Dai H, He YD, van't Veer LJ, Bartelink H, Rijn M van de, Brown PO, Vijver MJ van de: **Robustness, scalability, and integration of a wound-response gene expression signature in predicting breast cancer survival.** *Proc Natl Acad Sci USA* 2005, **102**:3738-3743.
- Bussemaker HJ, Li H, Siggia ED: **Regulatory element detection using correlation with expression.** *Nat Genet* 2001, **27**:167-171.
- Conlon EM, Liu XS, Lieb JD, Liu JS: **Integrating regulatory motif discovery and genome-wide expression analysis.** *Proc Natl Acad Sci USA* 2003, **100**:3339-3344.
- Das D, Banerjee N, Zhang MQ: **Interacting models of cooperative gene regulation.** *Proc Natl Acad Sci USA* 2004, **101**:16234-16239.
- Beer MA, Tavazoie S: **Predicting gene expression from sequence.** *Cell* 2004, **117**:185-198.
- Das D, Nahle Z, Zhang MQ: **Adaptively inferring human transcriptional subnetworks.** *Mol Syst Biol* 2006, **2**:0029.
- Smith AD, Sumazin P, Xuan Z, Zhang MQ: **DNA motifs in human and mouse proximal promoters predict tissue-specific expression.** *Proc Natl Acad Sci USA* 2006, **103**:6275-6280.
- Teschendorff AE, Journee M, Absil PA, Sepulchre R, Caldas C: **Elucidating the altered transcriptional programs in breast cancer using independent component analysis.** *PLoS Comput Biol* 2007, **3**:e161.
- Tonghai R, Idelman G, Nordgard SH, Cui W, Jacobs JL, Haggerty CM, Chanock SJ, Borresen-Dale AL, Livingston G, Shaughnessy P, Chiang CH, Kristensen VN, Bilke S, Gardner K: **Transcriptional networks inferred from molecular signatures of breast cancer.** *Am J Pathol* 2008, **172**:495-509.
- Matys V, Kel-Margoulis OV, Fricke E, Liebich I, Land S, Barre-Dirrie A, Reuter I, Chekmenev D, Krull M, Hornischer K, Voss N, Stegmaler P, Lewicki-Potapov B, Saxel H, Kel AE, Wingender E: **TRANSFAC and its module TRANSCOMP: transcriptional gene regulation in eukaryotes.** *Nucleic Acids Res* 2006, **34**:D108-D110.
- Vlieghe D, Sandelin A, De Bleser PJ, Vlemingck X, Wasserman WW, van Roy F, Lenhard B: **A new generation of JASPAR, the open-access repository for transcription factor binding site profiles.** *Nucleic Acids Res* 2006, **34**:D95-D97.
- Friedman N, Lital M, Nachman I, Pe'er D: **Using Bayesian networks to analyze expression data.** *J Comput Biol* 2000, **7**:601-620.
- Pan KH, Lih CJ, Cohen SN: **Effects of threshold choice on biological conclusions reached during analysis of gene expression by DNA microarrays.** *Proc Natl Acad Sci USA* 2005, **102**:8961-8965.
- Loh YH, Wu Q, Chew JL, Vega VB, Zhang W, Chen X, Bourque G, George J, Leong B, Liu J, Wong KY, Sung KW, Lee CW, Zhao XD, Chiu KP, Lipovich L, Kuznetsov VA, Robson P, Stanton LW, Wei CL, Ruan Y, Lim B, Ng HH: **The Oct4 and Nanog transcription network regulates pluripotency in mouse embryonic stem cells.** *Nat Genet* 2006, **38**:431-440.
- Hallikas O, Palin K, Sinjushina N, Rautiainen R, Partanen J, Ukkonen E, Taipale J: **Genome-wide prediction of mammalian enhancers based on analysis of transcription-factor binding affinity.** *Cell* 2006, **124**:47-59.
- Storey JD, Tibshirani R: **Statistical significance for genomewide studies.** *Proc Natl Acad Sci USA* 2003, **100**:9440-9445.